

UNCLASSIFIED

Defense Technical Information Center
Compilation Part Notice

ADP010492

TITLE: Integrated Flight Mechanic and Aeroelastic
Modelling and Control of a Flexible Aircraft
Considering Multidimensional Gust Input

DISTRIBUTION: Approved for public release, distribution unlimited

This paper is part of the following report:

TITLE: Structural Aspects of Flexible Aircraft
Control [les Aspects structuraux du controle
actif et flexible des aeronefs]

To order the complete compilation report, use: ADA388195

The component part is provided here to allow users access to individually authored sections of proceedings, annals, symposia, ect. However, the component should be considered within the context of the overall compilation report and not as a stand-alone technical report.

The following component part numbers comprise the compilation report:

ADP010474 thru ADP010498

UNCLASSIFIED

INTEGRATED FLIGHT MECHANIC AND AEROELASTIC MODELLING AND CONTROL OF A FLEXIBLE AIRCRAFT CONSIDERING MULTIDIMENSIONAL GUST INPUT

Patrick Teufel, Martin Hanel, Klaus H. Well
Institute of Flight Mechanics and Control
Stuttgart University
Pfaffenwaldring 7a
70550 Stuttgart, Germany

Abstract

In this paper, the influence of gusts on the dynamics of a large flexible aircraft is analyzed, and an integrated flight and aeroelastic control law that reduces gust sensitivity is presented. The calculations are based on an integrated model that includes all 1st order couplings between flight mechanic and structural degrees of freedom. Uniform, 1-dimensional and multidimensional gust models are implemented and used for gust sensitivity analysis. For the example aircraft, the differences in gust sensitivity calculated with the 1-dimensional and multi-dimensional gust models are significant. Integrated attitude, stability augmentation, and aeroelastic control laws for longitudinal and lateral motion are designed using μ -synthesis. With the control laws, flight maneuvers do not excite elastic reactions, and the sensitivity to gusts is considerably reduced.

Nomenclature

B_{hh}	= modal damping matrix
k	= reduced frequency
K_{hh}	= modal stiffness matrix
L	= characteristic wave length for gust (2500 ft)
M_{hh}	= modal mass matrix
P_h	= modal applied aerodynamic forces (gust)
$Q(ik)$	= modal aerodynamic force coefficient matrix tabulated for reduced frequencies k
q	= state vector in generalized coordinates
x_j	= x location of aerodynamic panel
x_0	= reference value for aerodynamic coordinate system
u, v, w	= longitudinal, lateral and vertical velocity
p, q, r	= roll, pitch and yaw rate
w	= aerodynamic downwash
α, β, γ	= angle of attack, sideslip angle and flight path angle
γ	= dihedral angle
Φ	= mode shape matrix
ϕ, θ, ψ	= roll attitude, pitch attitude and heading
φ	= phase angle
Φ	= matrix of one dimensional spectrum function
Ψ	= matrix of two dimensional spectrum function
ξ_{si}, ξ_{so}	= symmetric and antimetric deflection of
ξ_{ai}, ξ_{ao}	inner and outer ailerons
ξ, η, ζ	= aileron, elevator and rudder deflection
ω	= frequency
Ω	= ω/V wave number

1 Introduction

Today's airlines are requesting bigger and more fuel efficient aircraft to reduce their operation costs. Consequently, fuselages and spans of new aircraft designs are getting longer, and the need to reduce structural weight reduces structural stiffness.

Both effects lead to more flexible aircraft structures with significant aeroelastic coupling between flight mechanics and structural dynamics, especially at high speed, high altitude cruise. To counteract gust and maneuver induced aeroelastic vibrations, which impair ride comfort and structural loads, active aeroelastic control strategies are investigated.

Using separate models for flight mechanics and aeroelastics (sufficient for the smaller and more rigid aircraft in service today) aeroelastic coupling cannot be described. Further, it is doubtful whether simple uniform or 1D gust models are still adequate for large aircraft. To address the former deficiency, integrated models describing both the flight mechanic and the aeroelastic behavior of flexible aircraft have been developed recently¹. The issues of gust modelling and active aeroelastic control are addressed here.

Calculations of gust loads are of major importance for the structural and aerodynamic layout of an airplane. Certification requirements due to discrete gusts as well as continuous gust loads have been developed. FAR 25² describes one dimensional (1D) 1-cos shape gust requirements. The FAA-ADS 53² report describes 1D continuous gust requirements, which are based on power spectral density PSD methods.

There always have been efforts to extend existing gust formulations to a more realistic modelling as the most widely used 1D gusts are the most abstract realization of real gusts, which will be random not only in one direction but in each direction. The energy distribution within gusts has already been described in the early 60s by Dryden and von Kármán. These gust spectra have been developed in 3D space, but in the later years only the 1D spectra have been used. Nevertheless, research on multidimensional formulations of gusts and the modelling of the induced aerodynamic forces is continuing. On the evaluation of multidimensional gust fields and the resulting airplane responses, most authors rely on cross-spectral formulations. Crimaldi³ describes a method for 2D gust modelling which is based on calculations of the cross-spectrum of a gust acting on single aerodynamic strips of panels along the longitudinal axis of the airplane. These gust cross-spectra depending on the lateral separation distance have been developed by Eichenbaum⁴ and are described by Bessel functions of the third kind.

The gust models described in this paper avoid the evaluation of cross-spectral density functions by applying directly 1D and 2D PSD functions to vertical and lateral gusts as in Etkin⁵. Starting from a very basic formulation gust models are step by step developed towards a fully multidimensional gust description, so that effects caused by the increase in accuracy of the models can be identified.

Conventional flight control systems are designed to assure good handling qualities and to eliminate the influence of elasticity, treating the aircraft as a rigid body. For ride comfort improvement, separate aeroelastic control loops have been implemented on some modern aircraft⁶. The flight control and

the aeroelastic control loops are then separated by dynamic filters. As rigid body dynamics and low frequency elastic modes get closer with increasing structural flexibility, separate design of stability augmentation systems and aeroelastic control loops becomes more difficult. Therefore, several recent studies^{1,7,8,9,10} have investigated integrated flight mechanic and aeroelastic control design. In this study, an integrated flight and aeroelastic control law for a heavy study four-engine civil transport aircraft at high-speed, high-altitude cruise is presented, and the influence of the integrated control law on gust sensitivity is analyzed.

2 Integrated aircraft model

Linearized integrated flight mechanic and aeroelastic models for different flight (20000ft to 30000ft altitude and $Ma=0.4$ to $Ma=0.86$) and load (full and empty wing and trim tank) conditions are derived for the example aircraft. The modelling follows the procedure described by Schuler¹.

Structural Dynamics

The structural dynamics of the aircraft structure are analyzed using a detailed full-span FEM-model. A normal mode analysis is performed and the low-frequency elastic modes up to a frequency of about 20Hz are retained. Additional mode shapes for rigid body motion and control surface deflections are generated. Modal coordinates q (q_r for rigid body motion and q_e for elastic modes) are introduced and used to describe rigid body and structural dynamics:

$$\begin{aligned}\ddot{q}_r &= f(\dot{q}_r) + F_r^F + F_r^G + F_r^A \\ \ddot{q}_e &= -2\zeta_m \Lambda \dot{q}_e - \Lambda^2 q_e + F_e^F + F_e^A\end{aligned}\quad (1)$$

with $\Lambda = \text{diag}(\omega_i)$, modal damping coefficient ζ_m , (here $\zeta_m = 0.01$), aerodynamic forces F^A , thrust forces F^F and gravitational forces F^G . Displacement, velocity and acceleration of the structure in physical degrees of freedom (z, \dot{z}, \ddot{z}) are expressed in terms of modal coordinates by

$$z = \Phi q, \quad \dot{z} = \Phi \dot{q}, \quad \ddot{z} = \Phi \ddot{q}, \quad (2)$$

where Φ is the mode shape matrix.

Aerodynamics

Steady and unsteady aerodynamic forces are calculated using the Doublet-Lattice method¹¹, as implemented in NASTRAN. The location of the 1570 boxes (each representing a doublet-singularity) is shown in Fig. 1. Aerodynamic force coefficients are calculated for 18 discrete reduced frequencies and tabulated in matrices $Q(ik)$. Linearized aerodynamic forces can then be written as

$$\begin{bmatrix} F_r^A \\ F_e^A \end{bmatrix} = \begin{bmatrix} Q_{rr}(ik) & Q_{re}(ik) \\ Q_{er}(ik) & Q_{ee}(ik) \end{bmatrix} \begin{bmatrix} q_r \\ q_e \end{bmatrix} + \begin{bmatrix} Q_{rg}(ik) \\ Q_{eg}(ik) \end{bmatrix} w_g \quad (3)$$

with Q_{re} and Q_{er} representing the cross-coupling between rigid-body and structural modes and Q_{rg} and Q_{eg} the forces due to gust vector inputs w_g . In the form of Eq. 3, aerodynamic forces can only be evaluated for harmonic oscillations at given discrete frequencies. For simulation purposes and control law design, the aerodynamic force description is therefore extended to the Laplace domain, approximated by a rational transfer function matrix and then transformed to the time

domain. For this study, the Minimum State Method of Karpel¹⁴ has been used to perform the approximation.

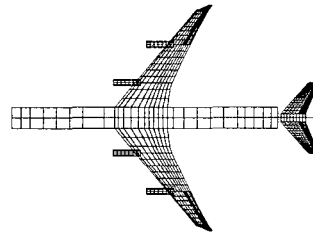


Fig. 1: Aerodynamic model (NASTRAN) - the lifting surface is discretized using 1570 doublet elements (boxes)

For the time-domain model, gusts are modelled as acting uniformly on the aircraft structure and separately on longitudinal and lateral motion. Then a (linear, time-invariant) state-space description of the (linearized) aircraft dynamics

$$\begin{aligned}\dot{x} &= Ax + Bu + Ew \\ z &= Cx + Du + Fw\end{aligned}\quad (4)$$

with control inputs u and (uniform) gust inputs w is derived^{12,13,1}. The uniform gust model however is too inaccurate an approximation for gust analysis. Therefore, in the sequence, more realistic gust models are discussed (sections 4 and 5). Finally it is analyzed how the controllers designed with the uniform gust model perform with respect to more realistic gust models (section 9).

3 Random turbulence models

For most evaluations turbulence is regarded as a random phenomenon. Its energy distribution has to be described in the 3D space.

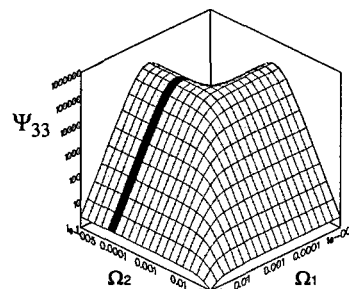


Fig. 2: 2D spectrum Ψ_{33} of vertical von Kármán turbulence

Considering vertical gusts for airplane, it is apparent that only variations in longitudinal and lateral direction will be significant and variations of gust velocity in vertical direction can be neglected as the airplane height is small in comparison to span and length. 2D spectra will therefore be appropriate. In this study, the von Kármán Spectrum¹⁵ is used to describe the energy distribution versus frequency. For vertical turbulence it is given by

$$\Psi_{33}(\Omega_1, \Omega_2) = \frac{16\sigma^2(\alpha L)^4}{9\pi} \cdot \frac{(\Omega_1^2 + \Omega_2^2)}{(1 + \alpha^2 L^2(\Omega_1^2 + \Omega_2^2))^{7/3}} \quad (5)$$

Results presented in this paper will be calculated with the appropriate 1D and 2D von Kármán spectra. Fig. 2 shows the 2D von Kármán spectrum. 1D spectra are obtained by integrating Eq. 5 with respect to Ω_2 . Wavenumber Ω_2 and Ω_1 will be discussed in section 5.

4 Standard 1D continuous gusts response

For 1D gust loads only changes of gust velocity in flight direction are considered, for vertical as well as for lateral gusts. One way to compute these gust forces is to assume a uniform gust velocity over the airplane. Gust forces are obtained that are equal to the generalized aerodynamic forces of the translational vertical and lateral rigid body modes. Standard gust calculations (NASTRAN) consider phase delay effects along the flight path. The gust field is assumed to be frozen (Taylor's hypothesis). Gust forces are related to a normal downwash at a specific aerodynamic box j by

$$P_h(\omega) = Q_{hj}(Ma, k)w_j(\omega), \quad (6)$$

where Q_{hj} relates downwash and modal aerodynamics forces and is available through NASTRAN. The downwash of a vertical gust which actually describes the phase delay is given by¹⁶

$$w_j(\omega) = \cos\gamma_j e^{-i\omega \frac{(x_j - x_0)}{V}}, \quad (7)$$

where the normal downwash on a aerodynamic box is proportional to the dihedral angle γ_j . For lateral gusts $\cos\gamma_j$ has to be replaced by $\sin\gamma_j$.

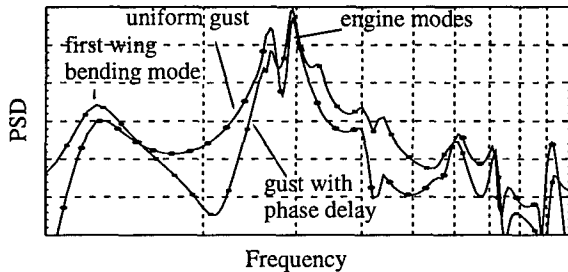


Fig. 3: PSD of acceleration of outer wing due to uniform vertical gust and gust with phase delay effects in flight path direction

The flutter equation in generalized coordinates is used for open loop simulations with applied forces:

$$\left[-M_{hh}\omega^2 + iB_{hh}\omega + K_{hh} - \left(\frac{1}{2}\rho V^2 \right) Q_{hh}(Ma, k) \right] q = P_h(\omega) \quad (8)$$

In this equation modal masses M_{hh} , damping B_{hh} and stiffness K_{hh} are real matrices, the matrix of modal aerodynamic forces Q_{hh} coefficients is complex. The result is obtained in modal coordinates. Displacement, velocity and acceleration of the structure in physical degrees of freedom can be computed with Eq. 2.

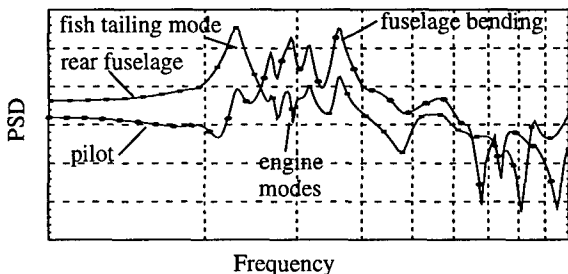


Fig. 4: PSD of acceleration of fuselage close to pilot and rear fuselage due to 1D lateral gust with phase delay

The RMS values of the response in physical coordinates are obtained by applying 1D gust spectra. Considering the phase

delay along the flight path is the first step towards a 2D gust model. The effect on the acceleration of the wing can be seen in Fig. 3. The evaluation of the response of the wing bending is used in most studies for the evaluation of the critical loads of an airplane. This might be in general true for smaller aircraft, but from Fig. 3 two important things can be seen: Phase delay changes the aircraft response, and there are modes beside symmetric wing bending at higher frequencies that will be considerably excited independent of gust model.

As to the response of an airplane to lateral gusts, it is obvious that the so called "fish tailing" mode and "fuselage bending" mode at higher frequency should be considered. The "fish tailing" mode results in high accelerations in the rear fuselage of the airplane and small loads at the front fuselage, see Fig. 4. For clarity: response of uniform gust is not depicted.

5 Multidimensional continuous gust response

Gust calculations for multidimensional continuous gusts are based on the method described by Etkin⁵. It differs from the 1D continuous gust in that there is an additional variation along the span. The gust velocity is varying along the flight direction as before and is "wavy" over the airplane.

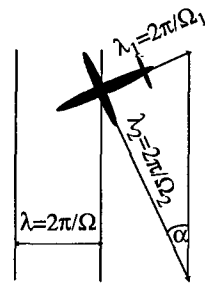


Fig. 5: Aircraft flying through a 2D vertical gust field

For the vertical gust case a 2D gust field is obtained, where the downwash is dependent on wave numbers $\Omega_1 = \omega/V$ and Ω_2 . Eq. 7 is modified:

$$w_j = \cos\gamma_j e^{i(\Omega_1(x_j - x_0) + \Omega_2 y_j)} \quad (9)$$

It can be seen that the second wave number Ω_2 results in a different phase of the downwash compared to the 1D gust assumption. Assuming a fixed proportion of Ω_2 and Ω_1 the situation can also be described by the airplane flying over a 1D gust field with an angle α , see Fig. 5. Lateral gusts are implemented similar to vertical gusts. By implementing the dependence on Ω_2 Eq. 8 is extended to a 2D transfer function. As an example the acceleration of the wing for different values of Ω_2 is presented. It can be shown that dependent on each characteristic mode, the second wave number Ω_2 yields higher or lower accelerations. Additionally, it has to be mentioned that because of the phase delay the response of the left and right side of the airplane will be different. Similar to the 1D-case the response has been multiplied with the 2D-spectrum. Neglecting longitudinal gusts it has been shown⁵ that the total RMS response for isotropic turbulence is given by the uncorrelated response of vertical and lateral gust. Therefore the spectra for lateral and vertical motion can be computed separately and added:

$$\Psi_{x_i x_i}(\Omega_1, \Omega_2) = |X_{iv}|^2 \Psi_{vv}(\Omega_1, \Omega_2) + |X_{iw}|^2 \Psi_{ww}(\Omega_1, \Omega_2) \quad (10)$$

In this equation $\Psi_{x_i x_i}$ is the 2D spectrum response of a selected physical degree of freedom x_i . X_{iv} is the response due to unit gust input.

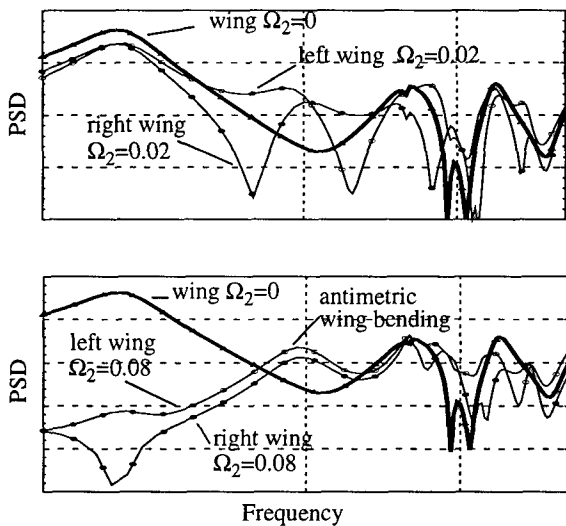


Fig. 6: PSD of acceleration of outer wing due to 2D vertical gust for $\Omega_2=0.02$ and $\Omega_2=0.08$

To compare these results with the 1D case we need

$$\Phi(\Omega_1) = \int_{-\infty}^{\infty} \Psi_{x_i x_i}(\Omega_1, \Omega_2) d\Omega_2. \quad (11)$$

With this equation the acceleration of the wing and of the outer engine due to 1D and 2D gust input is compared and presented in Fig. 7.

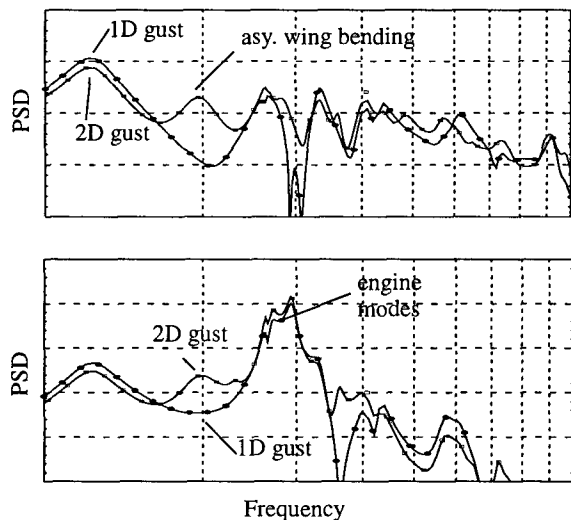


Fig. 7: PSD of vertical wing and lateral outer engine acceleration for 1D and 2D gust input

It can be seen that the 2D formulation leads to lower accelerations for the first wing bending mode. Due to the antimetric phase delay antimetric modes are excited, which can clearly be seen for the first antimetric wing bending mode. This antimetric response of the first wing bending explains the reduction in the symmetric wing bending, as the 1D spectrum with $\Omega_2=0$ puts too much emphasis on the first wing bending mode. In contrast to the first wing bending mode, there are modes whose response can increase for the 2D gust formulation. The reason is that based on the phase delay there are situations when the gust shape over the wing is equal to a characteristic wing bending form and will therefore amplify the response at this fre-

quency. As at higher frequencies gust spectra become very small, only the first number of elastic modes will lead to PSD values that are used for evaluation.

Adding lateral gusts to the response according to Eq. 10 causes a slight increase of loads on surfaces that are mainly affected by vertical gusts (see Fig. 8). For antimetric modes (“fish tailing”) the situation will be vice versa.

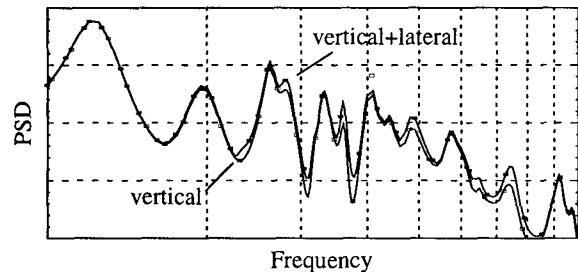


Fig. 8: PSD of vertical acceleration of outer wing due to vertical 2D gusts alone and a combination of vertical and lateral 2D gusts

6 Open loop system analysis

With all models based on NASTRAN frequency domain aerodynamics, frequency responses are the natural choice for aircraft dynamics analysis and offer the most accurate results. Further advantages are the possibility to clearly identify the influence of individual elastic modes, to assess the influence of random disturbances (such as gusts) and to readily draw conclusions for control design (stability margins etc.). While frequency responses could also be obtained from the linear state-space models (Eq. 4), those shown below have been calculated by directly solving the flutter equation (see Eq. 8), thus avoiding errors resulting from the transformation to the time-domain.

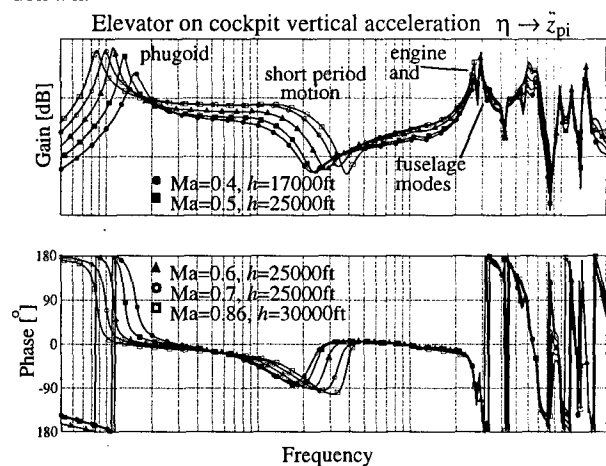


Fig. 9: Cockpit vertical acceleration frequency response to elevator input for different flight conditions

Fig. 9 shows the transfer function from elevator to cockpit vertical acceleration for different flight conditions. As expected from rigid-body flight mechanics, the gain amplitude increases with dynamic pressure, the phugoid frequency decreases, and the frequency of the short period motion increases with air speed. In the aeroelastic frequency range, the gain response shows the influence of dynamic pressure on amplitude, while phase response is not much affected by changes in flight condition. For changes in load condition, however, the situation is different. The load distribution (fuel and payload) strongly

influences the dynamic behaviour of the elastic structure and consequently aeroelastic coupling. Fig. 10 shows the frequency response for three different load conditions at constant flight condition. While changes in elastic mode shapes and frequencies are not unexpected (wing bending frequency should increase with fuel consumption), strong changes in damping (maximum amplitudes) and phase response are also observed.

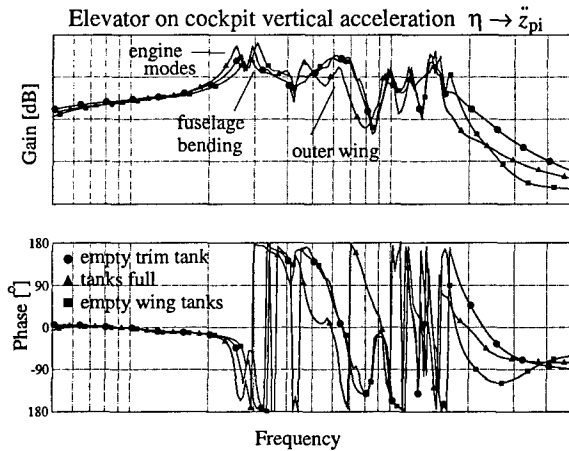


Fig. 10: Cockpit vertical acceleration frequency response to elevator input for different load conditions

A fixed gain control design therefore faces a robustness challenge in both the low-frequency range (rigid body dynamics changing mainly with flight condition) and the high-frequency range (aeroelastics changing mainly with load condition). With the low-frequency elastic modes being close to the short period mode, (the 1st wing bending mode is not visible in Figs. 9 and 10) strong coupling between rigid body and structural dynamics is observed.

Under these premises, the aforementioned difficulties associated with separate flight and aeroelastic control and the advantages offered by integrated control are evident.

7 Control design for integrated flight and aeroelastic control

Actuators

The integrated control law commands the conventional control surfaces for primary flight control, i.e. elevator, rudder, and inner and outer ailerons. While Schuler¹ assumes symmetrically deflected inner ailerons to be available in the longitudinal motion, in this study symmetric inner and outer aileron deflection is made available, however restricted to low authority aeroelastic control purposes.

Sensors

As all physically realizable sensor signals contain both rigid body and elastic motion, sensor number and position is an important consideration. Kubica and Livet⁸ and Ward and Ly⁷ use the signals of the conventional aircraft sensor platform. In this study, roll attitude ϕ and pitch attitude θ , roll, pitch and yaw rate (p, q, r), vertical and lateral acceleration are assumed to be measured by a sensor platform in the forward fuselage section. As in Schuler¹, additional accelerometers at different points of the aircraft structure are assumed to be available. They are placed at positions where low-frequency signals are dominant (providing for a physical low-pass filter) using a sensor placement strategy¹⁷. Vertical acceleration at a mid-wing

position and lateral acceleration at inner and outer engines are retained for both longitudinal and lateral control. Lateral acceleration at a rear fuselage position is added for lateral control.

Model reduction

As the linearized integrated model (see section 2) features a high number of states (e.g. 103 states for the longitudinal motion) an order reduction is required to derive a control design model. A 30-state reduced order model is obtained by applying a combination of balanced truncation and balanced condensation model reduction techniques¹⁸.

Choice of the Design Method

μ -synthesis^{19,20} has been chosen for control design for several reasons. Since the aircraft model is based on frequency-domain aerodynamics, frequency domain control design is advantageous, as important time-domain model characteristics, such as pole positions do not directly relate to the physical modelling process but result from the transformation of the frequency domain model to the time domain. The interpretation of short period frequency and damping for example is not possible in terms of short-period-pole-position alone, because the influence of aerodynamic lag-states has to be considered.

A MIMO control design method has been selected, as combined control surface actuation is much more effective for aeroelastic control than separate control loops for each control input, given the position of elevator and ailerons on the aircraft structure. With 30-state control design models, the availability of numerically reliable algorithms for H_∞ - optimization / μ -synthesis is another important consideration. Closed loop shaping^{21,22} has been chosen for setting up the H_∞ - optimization problem for its flexibility in translating design specifications into weighting functions.

The design process follows the procedure outlined in Ref. 10. The C^* combination of pitch rate and vertical acceleration ($C^* = q - \ddot{z}/V$) is chosen as control variable for the longitudinal motion. A proportional-integral control characteristic is achieved by adding the integral of C^* , C_i^* as an additional measurement. Accordingly, in the lateral motion, roll rate p is the control variable and roll angle ϕ is added for PI-control.

Command tracking, vibration reduction, aeroelastic damping increase, control effort, disturbance attenuation, and gust sensitivity are considered for nominal performance in the design by including and weighting the corresponding transfer functions in the performance index for H_∞ - control. As the more sophisticated gust models described in this article are not available for (state-space-model-based) control design, the gust sensitivity objectives are formulated using the uniform gust approach. In a robust performance formulation, robustness is demanded against changes in the aeroelastic frequency and damping parameters and strengthened in several μ -synthesis design iterations. The μ -synthesis design is executed using the *Xmath*-Software package.

The resulting 40th-order longitudinal controller features relatively high low-frequency gains for pitch rate and C^* feedback to elevator, nearly no low-frequency aileron activity and a rapidly decreasing control effort in the frequency range of the elastic modes. Acceleration measurements are mainly used for aeroelastic control purposes in the lower frequency range. Using Hankel norm optimal model reduction²³, a controller order reduction to 26 states can be performed without significant performance losses. High-frequency control gain attenua-

tion however is lowered. If the controller order is further reduced, performance rapidly deteriorates. In the lateral motion, roll rate and roll angle feedback on ailerons and yaw rate and sideslip (estimated from lateral acceleration) feedback on rudder dominate the integrated control law as expected. Again, the feedback of the acceleration measurements is principally used for aeroelastic control in the low aeroelastic frequency range. Model reduction techniques are applied to reduce the controller order (to 26 states).

8 Closed loop system analysis

In this section, an analysis of the closed loop aircraft dynamics is presented. The discussion is intended to give an overview over the different performance objectives considered for μ -synthesis. For the sake of brevity, it is restricted to the longitudinal motion. The results achieved with the lateral control law are similar to previous results¹⁰. Robustness to system changes, however, has been increased considerably by using μ -synthesis instead of standard H_∞ control.

The robust integrated flight and aeroelastic controller considerably increases the damping of the low-frequency elastic modes as shown by the comparison of open and closed loop pole locations in Fig. 11. Damping increase is 40 to 400% for the first 6 elastic modes.

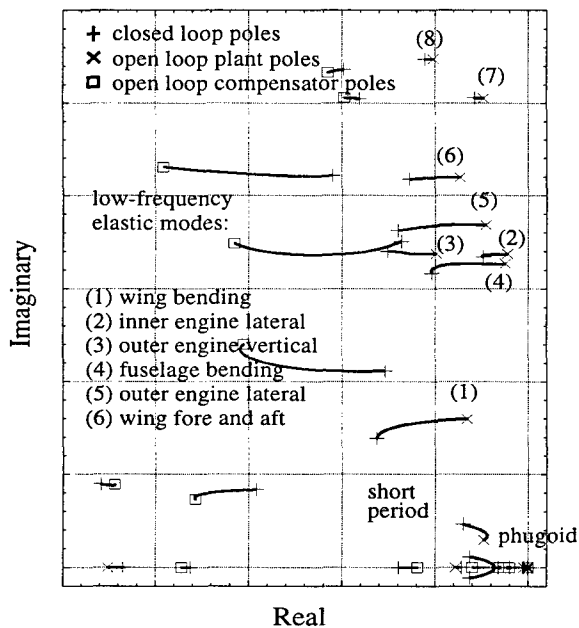


Fig. 11: Pole shifting - longitudinal control; final μ -controller on linearized plant model, Mach=0.86, $h=30000$ ft; plant pole damping is increased, while compensator (observer) poles are shifted to the right

For geometric reasons it could be expected that the damping of wing and engine modes is mainly due to the availability of symmetric aileron control input, whereas the damping of fuselage bending modes is achieved by elevator activity. While this was generally confirmed in the design process, coordinated control surface deflection enhances performance. For flight and load conditions beyond the design case, the damping increase achieved with the robust fixed gain controller in the loop and control performance in general decreases. Although, in the present case, a damping increase can be achieved for all flight and load conditions, the limits of robust fixed gain control for changing flight conditions are evident.

The closed loop time response to a 1s - pulse command $\dot{\gamma}=0.02^\circ/s$ and a 3.5° symmetric aileron disturbance impulse at $t=6s$ is shown in Fig. 12 (empty symbols).

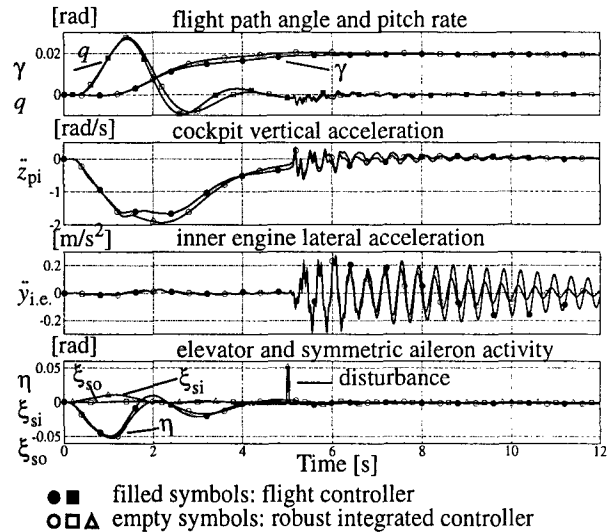


Fig. 12: Closed loop response comparison of a flight controller and the integrated flight and aeroelastic controller

For an assessment of the robust integrated controller, the time response of a simple C^* -flight controller is shown in comparison (filled symbols). Command tracking is equally fast for both controllers, with a somewhat lower short period frequency for the integrated controller.

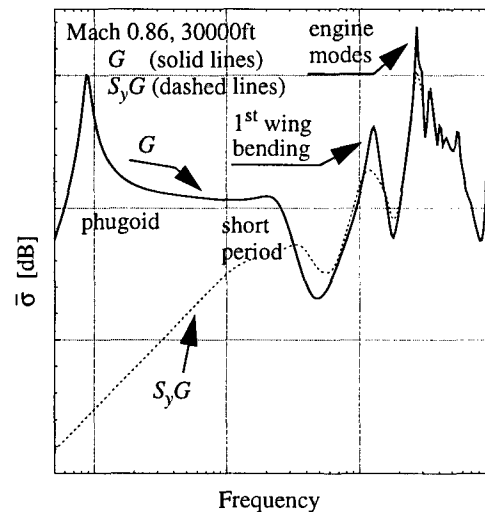


Fig. 13: Open and closed loop sensitivity to input perturbations - μ -controller longitudinal motion; Singular values of G and S_yG ; Sensitivity to input disturbances is reduced in the frequency range of controller operation;

The control effort of the integrated control law is based mainly on elevator. Low amplitude inner and outer aileron deflections are used for aeroelastic damping (but not for direct lift control).

While command tracking excites practically no elastic vibrations, the disturbance impulse causes aeroelastic vibrations. It can be seen that the integrated controller rapidly damps these vibrations, especially in the fuselage, but also at the inner engine. The handling qualities achieved with this controller are significantly improved over previous results¹⁰.

Input sensitivity

The singular values of the transfer matrix from the control (internal) inputs to the measurement (internal) outputs are calculated for both the open loop (G) and the closed loop system ($S_y G$) to analyze the sensitivity to input perturbations.

Fig. 13 shows the singular value diagram for the design flight and load condition for rigid body and elastic mode frequencies. It can be seen that the input disturbance sensitivity is considerably reduced in the frequency range of the phugoid and short-period motion, the lightly damped engine modes, and the fuselage bending mode. The input sensitivity in the range of higher frequency elastic modes is not affected by the control law. This observation confirms the conclusions drawn from the pole-shifting analysis.

9 Closed loop gust sensitivity

In this section, a detailed analysis of closed loop performance with respect to gusts is presented. In the first run, the uniform gust models used for control design and the NASTRAN 1D gust model (standard for smaller aircraft) are employed. In a second analysis run, the 2D gust model of section 5 is employed.

Gust sensitivity analysis using 1D gust models

For the gust sensitivity analyses of the first run, a 1D von Kármán gust spectrum¹⁵ is used.

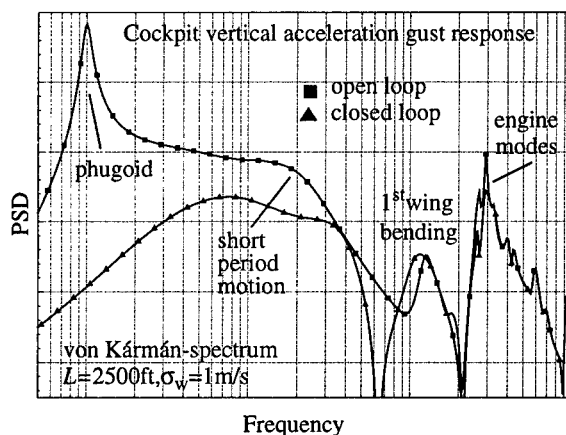


Fig. 14: 1D vertical gust response - vertical acceleration in the cockpit; open and closed loop sensitivity, Mach 0.7, $h=25000\text{ft}$, μ -controller; the gust sensitivity in the frequency range of the rigid body motion is reduced

Fig. 14 and 15 compare the open and the closed-loop cockpit vertical acceleration gust responses. As expected, a sensitivity reduction can be observed in the frequency range of the rigid body motion. Further, the integrated flight and aeroelastic controller achieves a significant reduction of the acceleration associated with engine and fuselage modes over the entire aircraft structure. The vertical gust-induced acceleration associated with e.g. the 1st wing bending mode is significantly reduced on the wing of the aircraft while no improvement (or even a deterioration) can be detected in the cockpit.

The influence of the controller on gust sensitivity is essentially similar for both the uniform gust model used for design and the 1D standard gust model, although the quantitative results differ.

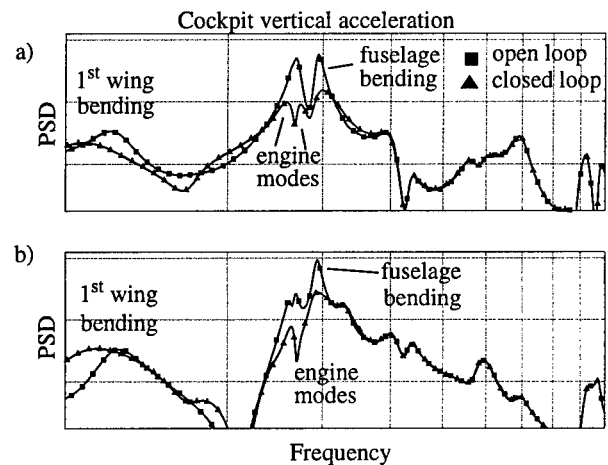


Fig. 15: Open and closed loop sensitivity to vertical gusts; a) uniform gust model; b) 1D gust model; von Kármán spectrum; μ -controller longitudinal motion, $Ma=0.7$, $h=25000\text{ft}$; the gust sensitivity reduction in the range of engine and fuselage modes is significant, independently of the gust model employed

The same analysis is performed for the lateral control law. Fig. 16 shows the cockpit lateral acceleration response to a von Kármán spectrum - based 1D lateral gust input for the open and the closed-loop system. Here the reduction in gust sensitivity achieved by the controller does not fulfill the expectations.

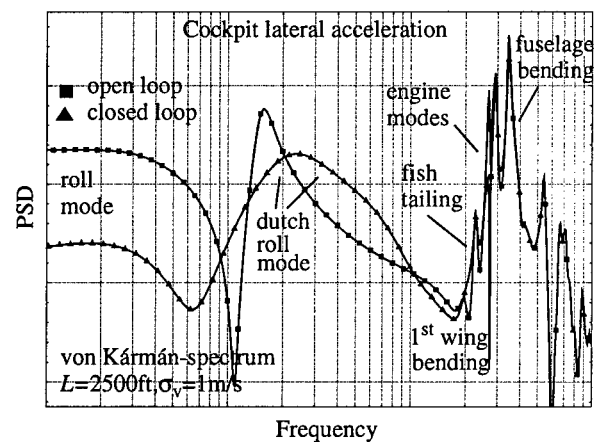


Fig. 16: 1D lateral gust response - lateral acceleration in the cockpit; open and closed loop sensitivity, $Ma=0.7$, $h=25000\text{ft}$, μ -controller; the gust sensitivity in the rigid-body mode frequency range is reduced;

While the gust sensitivity in the frequency range associated with the dutch roll mode is somewhat reduced and shifted to higher frequencies (as dutch roll frequency is increased), the sensitivity in the aeroelastic range is reduced only for some modes.

Fig. 17 shows the detailed results for both the uniform and the 1D gust models. It can be noted, that the significant reduction of the sensitivity peak associated with the fuselage bending mode in the case of uniform gusts is not achieved for 1D gusts. As the difference in phase between uniform and 1D lateral gusts unfolds over the length of the fuselage, it is not surprising that the fuselage bending mode is the most affected. Regarding the engine modes, the larger sensitivity reduction can be observed for the 1D gust model. For the fish-tailing mode, the

controller produces no improvement for uniform and even a deterioration for 1D gusts.

Therefore further research should concentrate on improving the performance with respect to fish-tailing. Further, it is expected that using the 1D gust model for control design will improve the achievable sensitivity reduction, especially with respect to fuselage bending.

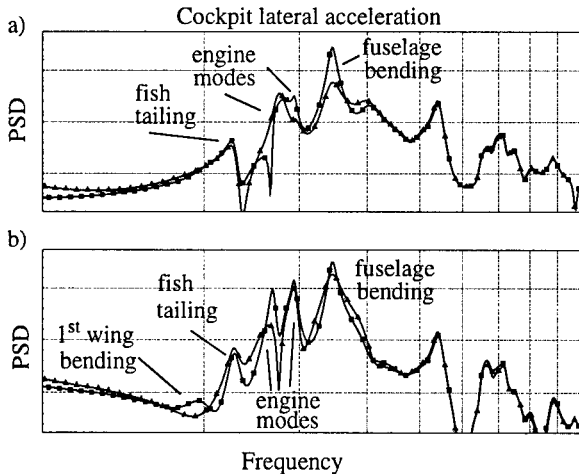


Fig. 17: Open and closed loop sensitivity to lateral gusts; a) uniform gust model; b) 1D gust model; μ -controller lateral motion, $Ma=0.7$, $h=25000ft$; sensitivity reduction depends strongly on the gust model

Gust sensitivity analysis using the 2D gust model

In the analysis run, the 2D gust model described in section 5 is employed to compare the open and closed loop gust sensitivity. Only the longitudinal controller is implemented.

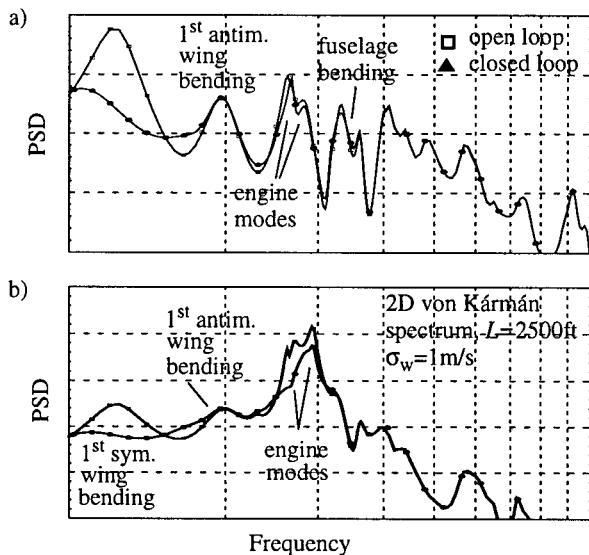


Fig. 18: Open and closed loop gust sensitivity to vertical gusts; 2D gust model; longitudinal μ -controller; a) PSD for outer wing vertical acceleration; b) PSD for outer engine lateral acceleration;

Fig. 18a shows the open and closed loop outer wing vertical acceleration PSDs. The outer engine lateral acceleration PSDs are given in Fig. 18b. The reduction of the sensitivity peaks associated with the symmetric modeshapes corresponds to the reduction observed for the 1D gust model. The increased

damping of the wing bending and engine modes entails a gust sensitivity reduction.

Naturally, the longitudinal controller cannot reduce the excitation of antimetric modeshapes. Clearly, for the example aircraft, lateral aeroelastic control action is required for vertical gust sensitivity reduction. It should be noted however, that by considering (uniform) roll gusts for lateral control design, the influence of vertical gusts on the lateral motion has already been partly accounted for.

10 Conclusion

In this paper the response of a large aircraft to gust input has been evaluated. For the analysis, a high fidelity structural and aerodynamic model that also represents aerodynamic coupling between rigid body and structural modes is employed. Using gust models of different accuracy and complexity (uniform, 1D, 2D, vertical and lateral), it is shown that aircraft reaction can diverge significantly for large aircraft.

Aeroelastic vibrations of the aircraft are considerably excited by vertical and lateral gusts. Therefore, realistic gust models that describe the distribution of the gust over the aircraft structure are required. From the comparison of uniform and 1D gust responses in the aeroelastic frequency range (e.g. fuselage bending), it can be concluded that uniform gust approximations are inadequate for sensitivity analysis. This is especially true for large airplanes, where the delays between the gust effect at the front and the rear of the aircraft are more important.

Investigations often neglect the response of aircraft due to lateral gusts, which also lead to a considerable excitation of the airplane. In particular, the bending modes of the fuselage and the wing versus fuselage "fish tailing" mode have to be studied, as they cause high loads at the rear fuselage.

The implementation of 2D gust models adds new aspects to the problem, especially the response of the wing is further modified. Vertical gusts excite antimetric modes and the energy of the gust is distributed on more modes. This explains the PSD-reduction associated with the first wing bending mode. On the other hand there are modes whose response is amplified by a 2D gust. In particular, if the gust velocity distribution has the same form as certain mode shapes (e.g. higher order wing bending or engine modes), an amplification of the corresponding PSD results.

The closed loop system analysis (section 8) demonstrates that the integrated controller meets the formulated performance requirements. The comparison of open loop and closed loop gust induced acceleration PSD curves shows that aeroelastic control achieves a significant reduction. The use of uniform gust approximations for control design is not satisfactory, as the sensitivity reduction results are different for the uniform and the 1D gust models. In particular, 1D gust sensitivity peaks associated with fuselage bending modes cannot be reduced by the controller. This is not unexpected as the phase difference between uniform and 1D gust excitations is strongest over the length of the fuselage.

Therefore, future research should concentrate on developing a realistic time-domain gust formulation that can be employed for state-space-model-based control design. It is expected that this step will entail a significant improvement in the controller performance, especially with respect to the fuselage bending modes and the fish-tailing mode.

Parts of this study have been funded within the research project "Dynamik des flexiblen Flugzeugs" by the German Ministry of Research and Technology (FKZ 20A9503G).

References

- [1] Schuler, J., *Flugregelung und aktive Schwingungsdämpfung für flexible Großraumflugzeuge*, Dissertation Universität Stuttgart, 1997
- [2] Hoblit, F.M., *Gust Loads on Aircraft: Concepts and Applications*, AIAA Education Series, Washington, 1988, ISBN 0-930403-45-2
- [3] Crimaldi, J.P., Britt, R.T., Rodden W.P., *Response of B-2 Aircraft to Nonuniform Spanwise Turbulence*, Journal of Aircraft, Vol. 30, No. 5, Sept.-Oct. 1993
- [4] Eichenbaum F.D., *Evaluation of 3D-Turbulence Techniques for Designing Aircraft*, Air Force Flight Dynamics Lab. TR-74-151, Wright-Patterson AFB, OH, Oct. 1972
- [5] Etkin, B., *The Turbulent Wind and its Effect on Flight*, The AIAA Wright Brothers Lecture, 1980, UTIAS Review No. 44
- [6] Seyffarth, K. et al., *Comfort in Turbulence for a Large Civil Transport Aircraft*, Proceedings of the International Forum on Aeroelasticity and Structural Dynamics, Strasbourg, May 1993
- [7] Ward, G., Ly, U., *Stability Augmentation Design of a Large Flexible Transport Using Nonlinear Parameter Optimization*, Journal of Guidance, Control and Dynamics, Vol. 19, No. 2, March-April 1996, pp. 469-474
- [8] Kubica, F., Livet, T., *Flight Control Law Synthesis for a Flexible Aircraft*, Proceedings of the AIAA Guidance, Navigation and Control Conference 1994, Scottsdale, AIAA-94-3630-CP, pp. 775-783
- [9] Gregory, I.M., *Dynamic inversion to control large flexible transport aircraft*, AIAA GNC Conference, Boston, 1998, AIAA-98-4323
- [10] Hanel, M., *Integrated Flight and Aeroelastic Control of a Flexible Transport Aircraft*, AIAA GNC Conference, Boston, 1998, AIAA-98-4297
- [11] Rodden, W.P., Albano E., *A Doublet-Lattice-Method for Calculating Lift Distributions on Oscillating Surfaces in Subsonic Flows*, AIAA Journal, Vol.7, No.2, Feb. 1969, pp. 279-285.
- [12] Rodden, W., Giesing, J., *Application of Oscillatory Aerodynamic Theory to Estimation of Dynamic Stability Derivatives*, Journal of Aircraft, Vol. 7, No. 3, June 1970, pp. 272 - 275
- [13] Rodden, W. et al., *Errata and Addenda to Application of Oscillatory Aerodynamic Theory to Estimation of Dynamic Stability Derivatives*, Journal of Aircraft, Vol. 21, No.1, January 1984, pp. 93 - 96
- [14] Karpel, M., *Minimum-State Unsteady Aerodynamic Approximations with Flexible Constraints*, Journal of Aircraft, Vol. 33, No.6, Nov.-Dec. 1996, pp. 1190-1196
- [15] Sawdy, D.T., *On the Two-Dimensional Atmospheric Turbulence Response of an Airplane*, Dissertation, University of Kansas, 1966
- [16] MSC NASTRAN, *Aeroelastic Analysis*, Manual, 1994
- [17] Hanel, M., Well, K.H., *Optimierte Sensorpositionierung zur Regelung elastischer Strukturen*, DGLR Jahrestagung, München, October 1997
- [18] Moore, B., *Principal Component Analysis in Linear Systems: Controllability, Observability and Model Reduction*, IEEE Transactions on Automatic Control, Vol. AC-26, No. 1, Feb. 1981, pp. 17-32
- [19] Packard, A., Doyle, J., *The Complex Structured Singular Value*, Automatica, Vol. 29, No.1, pp. 71-109, 1993
- [20] Balas, G. J., Doyle, J. C., Glover, K., Packard, A., Smith, R., *μ -Analysis and Synthesis Toolbox*, MUSYN Inc., and The MathWorks Inc., 1991.
- [21] Doyle, J., Glover, K., Khargonekar, P., Francis, B., *State-Space Solutions to Standard H_2 and H_∞ Control Problems*, IEEE Transactions on Automatic Control, Vol. 34, No. 8, August 1989, pp. 831-847
- [22] Glover, K., Doyle, J., *State-Space Formulae for all Stabilizing Controllers that Satisfy an H_∞ -Norm Bound and Relations to Risk Sensitivity*, System & Control Letters 11, 1988, pp. 167-172
- [23] K. Glover *All Optimal Hankel-Norm Approximations of Linear Multivariable Systems and their L^∞ -Error Bounds*, International Journal of Control, 1984, Vol.39, No.6, pp. 1115-1193